Wetting kinetics of water nano-droplet containing non-surfactant nanoparticles: A molecular dynamics study

Gui Lu,[1,2] Han Hu,[2] Yuanyuan Duan,[1,a)] and Ying Sun[2,a)]
[1]*Key Laboratory for Thermal Science and Power Engineering of MOE, Beijing Key Laboratory for CO_2 Utilization and Reduction Technology, Tsinghua University, Beijing 100084, People's Republic of China*
[2]*Department of Mechanical Engineering and Mechanics, Drexel University, Philadelphia, Pennsylvania 19104, USA*

(Received 26 July 2013; accepted 15 November 2013; published online 17 December 2013)

In this Letter, dynamic wetting of water nano-droplets containing non-surfactant gold nanoparticles on a gold substrate is examined via molecular dynamics simulations. The results show that the addition of non-surfactant nanoparticles hinders the nano-second droplet wetting process, attributed to the increases in both surface tension of the nanofluid and friction between nanofluid and substrate. The droplet wetting kinetics decreases with increasing nanoparticle loading and water-particle interaction energy. The observed wetting suppression and the absence of nanoparticle ordering near the contact line of nano-sized droplets differ from the wetting behaviors reported from nanofluid droplets of micron size or larger. © *2013 AIP Publishing LLC*. [http://dx.doi.org/10.1063/1.4837717]

Nanofluids, fluids containing suspensions of nanometer-sized particles, are a type of complex fluids designed to enhance thermal properties and/or reduce drag coefficients for applications ranging from electronics cooling to microfluidics, among others.[1–3] The suspended nanoparticles can significantly modify the transport properties of the base fluids, and the resulting nanofluids exhibit attractive properties such as high thermal conductivity and boiling heat transfer coefficient.[4,5] The wettability of nanofluids is of particular interest to microfluidic systems, in which surface tension plays an important role due to the relative small dimensions and high specific surface areas of these micro-devices.[6,7] Additionally, through wetting and particle deposition processes, nanofluids are widely used to functionalize substrates for desired surface morphologies and properties.[8]

The addition of nanoparticles makes the wetting kinetics of nanofluids more complicated compared with that of the base fluids, due to additional particle-particle, particle-substrate and particle-fluid interactions. The self-assembly of nanoparticles within the bulk liquid, at the solid-liquid and liquid-vapor interfaces, and/or in the vicinity of the contact line region greatly affects the wettability of nanofluids. Wasan and Nikolov[9] reported the enhancement of droplet spreading behavior, i.e., super-spreading of nanofluids of 8 nm micellar solution, 1 μm latex suspension, and 20 nm silica suspension. A solid-like ordering structure of nanoparticles was observed near the contact line region using interferometry. This solid-like ordering structure stemming from the settlement and assembly of nanoparticles gives rise to a structural disjoining pressure in the vicinity of the contact line. This excess pressure in turn alters the force balance near the contact line and enhances the spreading of nanofluids.[10–13] The super-spreading behavior of nanofluids was also reported in single-wall carbon nanotubes suspended in water[14] and aluminum–ethanol nanofluids.[15] The self-assembly of nanoparticles and the structural disjoining pressure induced super-spreading behavior of nanofluids were widely used to explain the enhancements in drop-wise evaporation[16,17] and critical heat flux of nanofluids.[18–21]

Although experimental observations[9,11] have been obtained for the effects of ordering of nanoparticles inside the micron-sized wedge-film near a contact line on the dynamic wetting of nanofluid droplets, no direct evidence has been provided for the fast spreading of nano-sized droplets containing nanoparticles, a process important to many nanofluidic devices and nanoporous membranes for water purification, for instance. Molecular-level simulations have been recognized as a powerful tool in examining transport phenomena of nanoparticles in a bulk liquid and at interfaces.[22–31] Self-assembly of nanoparticles of Lennard-Jones (LJ) type at fluid-fluid interfaces have been examined via molecular dynamics (MD) simulations.[22–27] Drazer *et al.*[28,29] and Li *et al.*[30] investigated the mobility of a single nanoparticle transporting in liquid (liquid argon or nitrogen) within a cylindrical nanochannel filled with nitrogen gas. Kim *et al.*[31] simulated the ring-like deposition of nanoparticles from a drying droplet using a Monte Carlo scheme. To date, no MD simulations have been reported for spreading of nanofluids on solid substrates. In addition, most MD simulations focused on nanofluids containing LJ particles in an LJ fluid, a system that is quite different from real nanofluids and is hence impossible to mimic important physical properties (e.g., surface tension, density, and viscosity) of nanofluids during wetting.

In this Letter, the dynamic wetting of water nano-droplet with non-surfactant gold nanoparticles on a gold substrate was studied using MD simulations with validated interatomic potentials. The results are compared first with the molecular kinetic theory (MKT).[32] The effects of particle volume fraction and particle wettability on the wetting kinetics and contact line mobility of nanofluids are examined. The surface tension of the nanofluids and the friction

[a)]Authors to whom correspondence should be addressed. Electronic addresses: yyduan@tsinghua.edu.cn, Tel./Fax: +86-10-62796318 and ysun@coe.drexel.edu, Tel./Fax: +1(215)895-1478.

between the nanofluid and substrate are calculated and compared with those of base fluids. The wetting behaviors of the present nano-sized nanofluid droplets are compared with those reported in literature based on nanofluid droplets of micron size or larger.

The cylindrical water droplets (diameter $d = 10$ nm, length $l = 1.64$ nm, 4500 water molecules) with four gold nanoparticle loading levels (number of nanoparticles $n = 0$, 9, 18, and 27, corresponding to particle volume fraction $\varphi = 0\%$, 3.43%, 6.77%, and 9.81%) spreading on a Au(100) surface ($61.35 \times 1.64 \times 1.64$ nm^3 fcc crystal total of 9600 gold atoms) at 300 K were simulated in this study. The gold nanoparticles ($0.8 \times 0.8 \times 0.8$ nm^3, 32 gold atoms per particle) were calibrated at 300 K and then absorbed spontaneously by a water droplet until the nanofluid system reached its minimum energy where the nanoparticles were randomly distributed inside the drop. The newly formed nanofluid droplets then spread on a Au(100) surface until the equilibrium contact angles were achieved. The four-point TIP4P-Ew water model[33] was used to describe the water-water interactions, where the particle-particle particle-mesh (PPPM) technique was used to compute the long-range Coulombic forces, and the SHAKE algorithm was applied to keep the water molecules rigid.[34] The embedded-atom method (EAM)[35] was applied for the gold-gold interactions, which occur among particle-particle, particle-substrate and substrate-substrate atoms. A 12-6 LJ potential with $\varepsilon = 0.05427$ eV, $\sigma = 3.1$ Å (Ref. 36) and a cut-off distance of 9 Å were used to describe the water-gold interactions, which yield an equilibrium water contact angle of $\theta_0 = 10^\circ \pm 1^\circ$, with errors obtained from using four different random velocity seeds for velocity initializations. The droplet spreading simulations were performed using LAMMPS[37] under NVT (N is the number of atoms, V is the volume, and T is the temperature) ensembles at $T = 300$ K. A time step of 1 fs was used in all cases.

Snapshots of a pure water droplet and three water-gold nanofluid droplets with particle volume fractions of 3.43%, 6.77%, and 9.81%, respectively, wetting on a Au(100) surface of 300 K at $t = 10$ ns are shown in Fig. 1 (water molecules are set transparent for a better visualization of the gold nanoparticles within the droplets from (b)–(d)). It can be

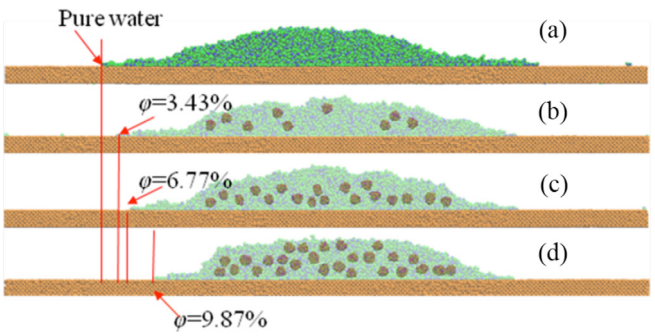

FIG. 1. Snapshots of nanoscale water droplet containing Au nanoparticles of various volume fractions spreading on a Au(100) surface of 300 K at $t = 10$ ns: (a) pure water; (b) nanofluid of $\varphi = 3.43\%$ ($n = 9$); (c) $\varphi = 6.77\%$ ($n = 18$); (d) $\varphi = 9.81\%$ ($n = 27$). Water molecules are made semi-transparent for a better visualization of nanoparticles within the droplets from (b)–(d)).

observed that the drop spreading radius decreases with the increasing nanoparticle volume fraction. No precursor film is observed for all cases. The addition of nanoparticles inhibits rather than enhances the spreading of nanoscale droplet during the nano-second spreading process. The nanoparticles distribute randomly in the droplet at $t = 10$ ns for nanofluids of all three particle loadings. No sign of solid-like ordering structure is observed in the vicinity of contact line during nanodroplet spreading, different from those reported in macroscopic experiments.[9] To examine the effect of self-assembly of nanoparticles, the diffusion time scale of nanoparticles was estimated by the Einstein diffusion theory,[38] where the diffusion coefficient is defined as $D = k_B T/3\pi\mu d$. Here, k_B is the Boltzmann constant 1.38×10^{-23} J/K, T is the temperature, μ is the viscosity of water, and d is the nanoparticle diameter. The diffusion time for one nanoparticle to move from the center of the droplet to the interface is $t_d = \pi R^2/D \approx 160$ ns at 300 K, much longer than the entire spreading process of approximately 10 ns. This implies that not enough time is available for nanoparticles to self-assemble into ordered structures near the contact line region during the spreading process. Consequently, the spreading enhancement of nanofluids due to the presence of structural disjoining pressure as a result of nanoparticle ordering is not valid mechanism in this study. Limited diffusion rate of nanoparticles in the contact line region as nanofluid spreads was also reported when 10 nm silica nanoparticles suspended in a polyethylene glycol solution.[39] It is noted here, the droplet sizes used in most nanofluid wetting studies were several millimeters in diameter,[9,11] corresponding to a much longer spreading time during which solid-like ordering structures of nanoparticles may occur.

In a microfluidic system, the dynamic spreading of a droplet is mainly controlled by the viscosity and surface tension of the fluid. To examine the effects of these two properties on dynamic spreading, the dimensionless drop spreading radius, $R' = R/R_0$, as a function of the dimensionless time $t' = \gamma t/\mu_{\text{eff}} R_0$ is plotted in Fig. 2. Here, R_0 is the initial drop radius prior to spreading, γ is the surface tension of water, and μ_{eff} is the effective viscosity of the nanofluid, calculated using $\mu_{\text{eff}} = \mu(1 + 2.5\varphi)$ to eliminate the effect of viscosity in droplet spreading kinetics. For fluids of equal surface tension, the R' versus t' curves are expected to collapse into one master curve.[40] However, as shown in Fig. 2, both the dynamics and equilibrium spreading radii decrease with the presence of nanoparticles and further decrease with the increasing nanoparticle volume fraction, indicating a change in surface tension of nanofluids with particle loading.

To evaluate the surface tension of nanofluids, two NVT systems, one with a nanofluid film of two free surfaces and the other with only a bulk nanofluid were simulated. The time-averaged excess energy of these two systems, $\langle E_w \rangle$-$\langle E_{w/o} \rangle$, led to the surface tension, $(\langle E_w \rangle$-$\langle E_{w/o} \rangle)/A_{\text{interface}}$, for pure water and nanofluids with different particle loadings. Here, the subscripts w and w/o denote with and without liquid-vapor interfaces, respectively. In MD simulations, surface tension can also be calculated from pressure based on the Young-Laplace equation[41] but is avoided here due to large pressure fluctuations. Table I summarizes the calculated liquid-vapor surface tensions based on the free energy method for pure water and

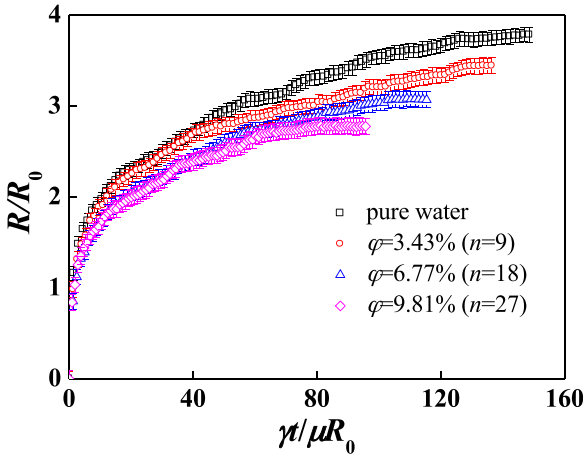

FIG. 2. Dimensionless spreading radius as a function of the dimensionless time for cylindrical water nanofluid droplets containing Au nanoparticles of volume fractions of 0%, 3.43%, 6.77%, and 9.81% on a Au(100) substrate. Error bars are obtained by using four different random velocity seeds for temperature initializations.

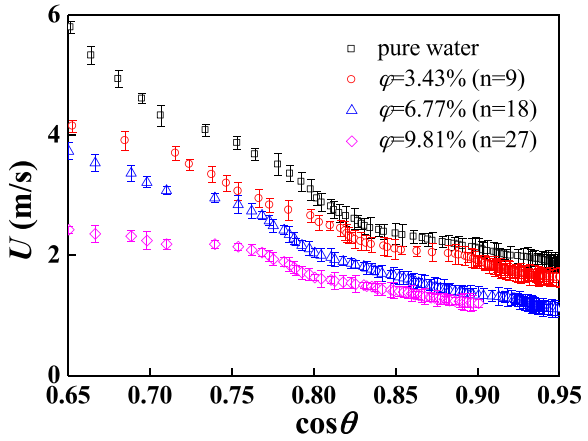

FIG. 3. The contact line velocity, U, as a function of $\cos\theta$ (θ is the dynamic contact angle) for water-gold nanofluid droplets with particle volume fractions of 0%, 3.43%, 6.77%, and 9.81%. Error bars are obtained by using 4 different random velocity seeds for temperature initializations.

nanofluids of $\varphi = 3.43\%$, 6.77%, and 9.81%, where error bars are obtained by using four different random velocity seeds for temperature initializations. For pure water, the calculated surface tension is $\gamma = 0.0679 \pm 0.0043$ N/m at $T = 300$ K, within 6% error compared with the experimental value of $\gamma = 0.072$ N/m.[42] As the nanoparticle loading increases, the surface tension of nanofluids increases from 0.1002 ± 0.0065 N/m for $\varphi = 3.43\%$ to 0.1175 ± 0.0075 N/m for $\varphi = 9.81\%$. The increase in surface tension of water droplet with non-surfactant nanoparticles was also reported by Tanvir *et al.*[43] and Moosavi *et al.*[44] as a result of the van der Waals forces between particles at the liquid-gas interface.

The spreading coefficient, $S = \gamma_{sv} - \gamma_{sl} - \gamma_{lv}$, where subscript s, l and v denote solid, liquid and vapor phases, respectively, is widely used to characterize the droplet spreading capacity and indicates the resultant force triggering the out-spreading motion of contact line. As the liquid-vapor surface tension increases with the increasing volume fraction of non-surfactant nanoparticles, the spreading coefficient S decreases, corresponding to a slower contact line velocity and a smaller equilibrium spreading radius. The wettability deterioration due to the increase in surface tension was also reported by Moffat *et al.*,[17] Kwok *et al.*,[45] and Chen *et al.*[46]

For wetting of a liquid droplet on a solid surface, models have been developed to connect wetting kinetics to relevant driving forces and dissipation mechanisms using the power-law form of the drop spreading radius, R, versus time t, i.e., $R \sim t^{\alpha}$, where α is determined by the specific dissipation mechanism. Alternatively, expressions connecting the contact line velocity U to the dynamic contact angle θ can be used to identify which mechanisms are dominant in determining contact line kinetics. Kinetic models for inert wetting include those identifying liquid viscous forces as the primary resistance to spreading, i.e., the hydrodynamic model,[47] as compared to those identifying molecular frication at the contact line as the dominant dissipation mechanism, i.e., MKT.[32] The hydrodynamic model gives $\alpha = 1/10$ for a spherical drop and $\alpha = 1/7$ for a cylindrical geometry and the MKT yields $\alpha = 1/7$ for spherical and 1/5 for cylindrical, respectively. In this study, the curve-fitted power α of the cylindrical water drop wetting on a Au(100) surface is 0.251, close to that of $\alpha = 1/5$ from the MKT. This result implies that the molecular adsorption and desorption of water to and from the Au(100) surface are very likely to be the dominant dissipation mechanism during wetting. In the MKT,[32] the relation of contact line velocity and dynamic contact angle gives, $U/\cos\theta \sim \gamma_{lv}/\zeta$, where ζ is the solid-liquid friction coefficient. Figure 3 illustrates $U \sim \cos\theta$ for nanofluid droplets with particle volume fractions of 0%, 3.43%, 6.77%, and 9.81%. Here, the dynamic contact angle θ is measured by linear fitting of the instantaneous drop radius of the first six layers of water molecules above the gold substrate surface. The results show good linearity ($R^2 > 0.989$) of $U \sim \cos\theta$ for $t > 3$ ns ($\cos\theta > 0.8$ corresponding to 36.9°, consistent with the validity of the MKT for wetting scenarios with a small contact angle). The slope attained from the linear fitting of $U \sim \cos\theta$ gives $\gamma_{lv}/\zeta = 5.294 \pm 0.258$ for nanofluids of particle loading up to ~10%. It is noted that, the calculated friction coefficient of pure water is 0.0143 Pa·s, consistent with the reported value of 0.01 Pa·s for water on a polyethylene terephthalate substrate.[48] Similar γ_{lv}/ζ ratios for pure water

TABLE I. Liquid-vapor surface tension of water and water-gold nanofluids of different volume fractions based on the free energy method.

	Pure water	$n = 9$	$n = 18$	$n = 27$
φ	0	3.43%	6.77%	9.81%
$\langle E_w \rangle$ (eV)	-1789.081 ± 3.343	-2841.828 ± 5.399	-3885.474 ± 8.548	-4943.323 ± 10.875
$\langle E_{w/o} \rangle$ (eV)	-1796.242 ± 3.481	-2853.841 ± 5.993	-3910.417 ± 7.820	-4969.034 ± 10.435
γ_{lv} (N/m)	0.0679 ± 0.0043	0.1002 ± 0.0065	0.1109 ± 0.0073	0.1175 ± 0.0075

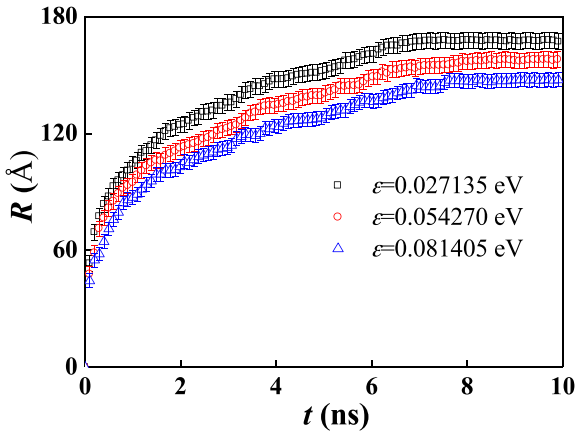

FIG. 4. The spreading radius as a function of spreading time for nanofluid droplets with different particle wettabilities for particle volume fraction of $\varphi = 9.81\%$. Error bars are obtained by using four different random velocity seeds for temperature initializations.

and nanofluids of various particle loadings (the standard deviation of 0.258) indicate that the solid-liquid friction coefficient increases with the increasing liquid-vapor surface tension. The MKT assumes that the viscous dissipation in a bulk liquid is negligible while focusing on the local dissipation in the vicinity of contact line so that the friction coefficient, ζ, is affected only by surface tension. A larger surface tension due to a higher non-surfactant nanoparticle volume fraction leads to a larger solid-liquid friction during the dynamic wetting process.

Figure 4 shows the effect of wettability of nanoparticles on the dynamic spreading of nanofluid droplets of $\varphi = 9.81\%$. Here, the wettability of nanoparticles is modified by changing the particle-water interaction energy ε (the wettability increases with increasing ε) while keeping ε of substrate-water the same. As expected, the droplet spreading kinetics slows down when the interaction between particles and water molecules increases, which can be attributed to the increases in both the surface tension and solid-liquid friction.

In conclusion, the dynamic spreading of water nano-droplets containing non-surfactant nanoparticles is examined via molecular dynamics simulations. The addition of non-surfactant nanoparticles hinders rather than enhances the droplet spreading kinetics during the nano-second process. The contact line velocity decreases with increasing nanoparticle volume fraction and particle-water interactions, as a result of increasing surface tension and solid-liquid friction and the absence of nanoparticle ordering in the vicinity of contact line. It is important to note that, in the present study, the diameter of the nano-droplets is only about ten times that of nanoparticles. Future studies will focus on exploring the threshold droplet size where nanoparticle ordering becomes significant and the surface tension is not significantly affected by the presence of nanoparticles.

The authors acknowledge financial support from NSFC (Nos. 21176133 and 51321002) and the U.S. National Science Foundation (Grant Nos. CAREER-0968927, DMR-1104835, and CMMI-1200385). Computational resources were provided by the Extreme Science and Engineering Discovery Environment (XSEDE) (Grant No. TG-CTS110056) and by Tsinghua National Laboratory for Information Science and Technology.

[1]U. S. Choi, *Developments and Application of Non-Newtonian Flows* (ASME, New York, 1995), Vol. FED 231/MD-Vol. 66, p. 99.
[2]S. K. Das, U. S. Choi, and H. E. Patel, Heat Transfer Eng. **27**, 3 (2006).
[3]H. S Ahn and M. H. Kim, J. Heat Transfer **134**, 024001–024002 (2012).
[4]V. Trisaksri and S. Wongwises, Renewable Sustainable Energy Rev. **11**, 512 (2007).
[5]S. Kakac and A. Pramuanjaroenkij, Int. J. Heat Mass Transfer **52**, 3187 (2009).
[6]P. G. de Gennes, Rev. Mod. Phys. **57**, 827 (1985).
[7]D. Bonn, J. Eggers, J. Indekeu, J. Meunier, and E. Rolley, Rev. Mod. Phys. **81**, 739 (2009).
[8]J. I. Brauman and P. Szuromi, Science **273**, 855 (1996).
[9]D. T. Wasan and A. D. Nikolov, Nature **423**, 156 (2003).
[10]K. Kondiparty, A. D. Nikolov, S. Wu, and D. T. Wasan, Langmuir **27**, 3324 (2011).
[11]K. Kondiparty, A. D. Nikolov, D. T. Wasan, and K. L. Liu, Langmuir **28**, 14618 (2012).
[12]K. L. Liu, K. Kondiparty, A. D. Nikolov, and D. T. Wasan, Langmuir **28**, 16274 (2012).
[13]M. J. Chaudbury, Nature **423**, 131 (2003).
[14]J. Shen, J. A. Liburdy, D. V. Pence, and V. Narayanan, J. Phys. Condens. Matter **21**, 464133 (2009).
[15]K. Sefiane, J. Skilling, and J. MacGillivray, Adv. Colloid Interface Sci. **138**, 101 (2008).
[16]K. Sefiane and R. Bennacer, Adv. Colloid Interface Sci. **147–148**, 263 (2009).
[17]J. R. Moffat, K. Sefiane, and M. E. R. Shanahan, J. Phys. Chem. B **113**, 8860 (2009).
[18]S. M. S. Murshed, C. A. Nieto de Castro, M. J. V. Lourenco, M. L. M. Lopes, and F. J. V. Santos, Renewable Sustainable Energy Rev. **15**, 2342 (2011).
[19]D. S. Wen, Int. J. Heat Mass Transfer **51**, 4958 (2008).
[20]S. J. Kim, I. C. Bang, J. Buongiorno, and L. W. Hu, Appl. Phys. Lett. **89**, 153107 (2006).
[21]K. Sefiane, Appl. Phys. Lett. **89**, 044106 (2006).
[22]S. F. Cheng and G. S. Grest, J. Chem. Phys. **136**, 214702 (2012).
[23]D. S. Frost and L. L. Dai, Langmuir **27**, 11339 (2011).
[24]M. Luo and L. L. Dai, J. Phys. Condens. Matter **19**, 375109 (2007).
[25]M. Luo, O. A. Mazyar, Q. Zhu, M. W. Vaughn, W. L. Hase, and L. L. Dai, Langmuir **22**, 6385 (2006).
[26]Y. Song, M. Luo, and L. L. Dai, Langmuir **26**, 5 (2010).
[27]D. S. Frost and L. Dai, J. Chem. Phys. **136**, 084706 (2012).
[28]G. Drazer, J. Koplik, A. Acrivos, and B. Khusid, Phys. Rev. Lett. **89**, 244501 (2002).
[29]G. Drazer, B. Khusid, J. Koplik, and A. Acrivos, Phys. Fluids **17**, 017102 (2005).
[30]Z. G. Li and G. Drazer, Phys. Fluids **20**, 103601 (2008).
[31]H. S. Kim, S. S. Park, and F. Hagelberg, J. Nanopart. Res. **13**, 59 (2011).
[32]T. D. Blake and J. M. Haynes, J. Colloid Interface Sci. **30**, 421 (1969).
[33]H. W. Horn, W. C. Swope, J. W. Pitera, J. D. Madura, T. J. Dick, G. L. Hura, and T. Head-Gordon, J. Chem. Phys. **120**, 9665 (2004).
[34]J. P. Ryckaert, G. Ciccotti, and H. J. C. Berendsen, J. Comput. Phys. **23**, 327 (1977).
[35]M. S. Daw, S. M. Foiles, and M. I. Baskes, Mater. Sci. Rep. **9**, 251 (1993).
[36]P. Schravendijk, N. Van der Vegt, L. D. Site, and K. Kremer, ChemPhysChem **6**, 1866 (2005).
[37]S. Plimpton, J. Comput. Phys. **117**, 1 (1995).
[38]A. Einstein, Ann. Phys. **322**, 549 (1905).
[39]Z. P. Liang, X. D. Wang, D. J. Lee, X. F. Peng, and A. Su, J. Phys. Condens. Matter **21**, 464117 (2009).
[40]A. Zosel, Colloid Polym. Sci. **271**, 680 (1993).
[41]A. E. Ismail, G. S. Grest, and M. J. Stevens, J. Chem. Phys. **125**, 014702 (2006).
[42]G. J. Gittens, J. Colloid Interface Sci. **30**, 406 (1969).
[43]S. Tanvir and Q. Li, Nanoscale Res. Lett. **7**, 226 (2012).
[44]M. Moosavi, E. K. Goharshadi, and A. Youssefi, Int. J. Heat Fluid Flow **31**, 599 (2010).
[45]D. Y. Kwok and A. W. Neumann, Colloid Surf., A **161**, 31 (2000).
[46]R. H. Chen, T. X. Phuoc, and D. Martello, Int. J. Heat Mass Transfer **54**, 2459 (2011).
[47]L. H. Tanner, J. Phys. D: Appl. Phys. **12**, 1473 (1979).
[48]T. D. Blake, J. Colloid Interface Sci. **299**, 1 (2006).